Macromolecules

ARTICLE

pubs.acs.org/Macromolecules

Fundamental Limitations on Ordered Electrohydrodynamic Patterning

Cindy Y. Lau and William B. Russel*

Department of Chemical and Biological Engineering, Princeton University, Princeton, New Jersey 08544, United States

Supporting Information

ABSTRACT: Studies have shown that electrohydrodynamic patterning (EHD) can produce ordered pillar arrays in polymer films at the micrometer scale in fewer processing steps than other techniques. This paper reports the limitation encountered in reducing the feature size, generally characterized by the fastest growing wavelength (λ_{max}), to submicrometer. An experiment designed to decrease λ_{max} well below a micrometer produced poorly ordered pillars that were considerably coarser than expected. Further experiments demonstrated that dielectric breakdown of the polymer limits the extent of feature size.

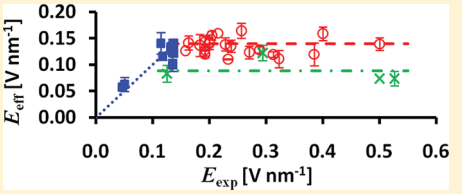

INTRODUCTION

Over the past few decades, submicrometer-sized features in thin films have gained importance and found many applications, motivating the development of cheap and fast methods to fabricate large arrays. Previous studies have shown that pillar arrays with micrometer-sized periods can be obtained via electrohydrodynamic patterning (EHD) of polymer films.[1−11] The typical pattern is hexagonally ordered[3−5] as shown in Figure 1a. Similar patterns at the submicrometer scale would have a range of applications, including photonic band gap materials for waveguides,[12] structural coloring and antireflective surfaces,[13] biomimetic materials with water-repellent surfaces,[14] and electrophoresis devices that sort macromolecules according to size and mobility.[15,16] Therefore, we are interested in producing patterns with submicrometer-sized features using EHD.

In EHD, the substrate consists of a polymer film spin-coated onto a silicon wafer, while the mask includes silicon dioxide spacers deposited onto another silicon wafer. The spacers maintain a gap above the polymer film when the substrate and the mask are pressed together. At a temperature above its glass transition temperature (T_g), an instability causes the polymer to flow in response to the voltage applied across the two silicon wafers, which act as electrodes. Schematics of the experimental setup are shown in Figure 2. A balance between the electrostatic force, the capillary force, and the viscous stresses ultimately results in a hexagonally ordered pillar array with a characteristic wavelength λ_{max}. A linear stability analysis predicts λ_{max} as a function of the applied voltage V, the film thickness h_0, the electrode separation H, surface tension γ, and dielectric constants ε and conductivities σ of the layers.[1−3] A smaller λ_{max} is expected with increasing V, decreasing h_0 (for $\varepsilon_2 > \varepsilon_1$, and vice versa) or decreasing H as shown experimentally by several groups.[4−8] One can also decrease γ or increase the dielectric constant of the top layer ε_2, for example, by replacing the air with an oligomer or polymer as shown by other groups.[9,11] Lastly, the dielectric constant ε_1 or conductivity σ of the polymer can be increased by incorporating gold nanoparticles or ions.[10] While these variations have decreased λ_{max}, the reported values generally range between about 1.6 μm to tens of micrometers and rarely, if ever, fall in the submicrometer range.

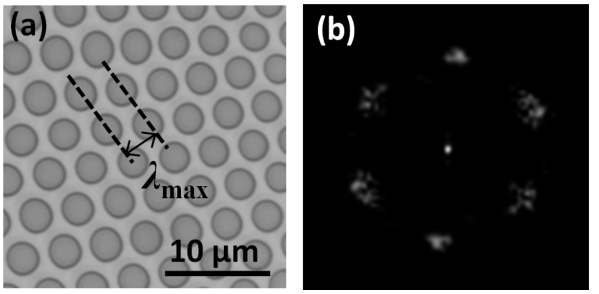

Figure 1. (a) An optical micrograph and (b) the fast Fourier transform (FFT) image of typical hexagonally ordered pillar patterns from EHD on a polymer−air bilayer. The interplanar distance between pillars is λ_{max}.

Submicrometer features replicating a patterned mask have been achieved with electrohydrodynamic patterning,[17,18] but we sought to reach that goal with a flat mask to avoid the more costly and slower photolithography required. Furthermore, we realized that dielectric breakdown in the air can limit the reduction of EHD feature size, as discussed in an earlier study[19] and investigated further in the first section of this paper.

In pursuit of submicrometer features, we combined a room-temperature ionic liquid (IL) with polymer films as described in the second section. Such an ionic liquid, a molten salt, does not break down dielectrically and minimizes the voltage drop across the top layer, thereby maximizing the voltage drop across the polymer film. The ionic liquid also offers a favorable interfacial

Received: April 28, 2011
Revised: July 14, 2011
Published: August 30, 2011

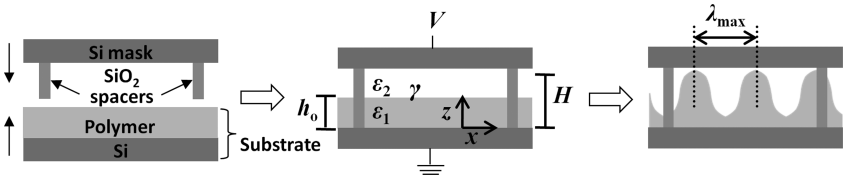

Figure 2. Schematics of the experimental setup, with V the applied voltage, ε_1 and ε_2 the dielectric constants of the polymer and top layer, respectively, γ the surface tension, h_0 the polymer film thickness, and H the electrode separation. The lateral and vertical coordinate systems are x and z, respectively.

tension, dielectric constant, and conductivity. Although aqueous electrolyte solutions provide these advantages, they vaporize at our experimental temperature ($T > T_g$ of polystyrene ~100 °C or T_g of poly(methyl methacrylate) ~106 °C[20]), whereas the IL has a very high decomposition temperature (~300 °C). While achieving submicrometer features as expected, we will show that the dielectric breakdown, now in the polymer, still limits the scale of the patterns.

EXPERIMENTAL SECTION

1. Materials. 1-Butyl-3-methylimidazolium tetrafluoroborate (BMI-BF_4), an ionic liquid, was purchased from Acros Organics. Poly(methyl methacrylate) (PMMA) and polystyrene (PS) of various molecular weights were purchased from Polymer Source, Inc. (M_w of 2, 31.8, and 62.5 kg mol^{-1} for PMMA and M_w of 2.1 and 76.5 kg mol^{-1} for PS). Polymer films of thicknesses between 16 and 147 nm were prepared by spin-coating polymer−toluene solutions onto silicon(100) wafers (Silicon Quest International) at various speeds. The thickness of the film was measured by an ellipsometer (L3W16 Gaertner Scientific).

To determine the appropriate molecular weight of polymer needed to create immiscible layers with BMI-BF_4, we measured the contact angle at 120 and 110 °C for PMMA and PS, respectively. The contact angle decreased quickly as an indication of polymer dissolution for low molecular weight polymers but remained constant for at least 3 h for PMMA63K (i.e., 62.5 kg mol^{-1})-(BMI-BF_4) or PS77K (i.e., 76.5 kg mol^{-1})-(BMI-BF_4). Therefore, we performed EHD on PMMA63K-(BMI-BF_4) and PS77K-(BMI-BF_4) bilayers.

2. Electrohydrodynamic Patterning (EHD). The mask for EHD was prepared by depositing silicon dioxide spacers of 81−278 nm, measured by a KLA-Tencor (P-15, KLA-Tencor), onto Si wafers via shadow mask lithography with an E-Beam Evaporator (DV-502A, Denton Vacuum). It was then coated with a monolayer of mold-release agent trichloro(1*H*,1*H*,2*H*,2*H*-perfluorooctyl)silane (97%, Aldrich) through vapor deposition. For the ionic liquid EHD experiments, thin silicon dioxide layers were predeposited on the silicon wafers to improve the adhesion of the mold-release agent to the mask.

PMMA2K (i.e. 2 kg mol^{-1}) films of 48 ± 3 nm and masks with 171 ± 2 nm spacers formed the polymer−air systems. The mask was pushed against the film at a constant pressure and a temperature of 130 °C. A dc power supply (1715A, BK Precision) provided constant voltages between −40 and 50 V across the electrodes and displayed the output current. The duration of the experiment was determined from the expected growth rate for pillars with λ_{max} separation. After the pillars formed at 130 °C, the system was cooled and separated at room temperature.

The EHD on a polymer−ionic liquid bilayer was similar except that a drop of BMI-BF_4 was placed on the polymer film before application of the mask. A function generator (DS 360, Stanford Research Systems, Inc.) supplied a voltage alternating at ω, which proved necessary to avoid oxidation of the ionic liquid. Our experiments covered a range of conditions (h_0 = 16−131 nm, H = 88−278 nm, V = 2−20 V, ω = 1−100 kHz, T = 102−110 °C). After separation from the mask, the bilayer was rinsed gently with water, which is totally miscible with BMI-BF_4 but immiscible with the polymer, and blown dry.

The pattern formed was imaged with an optical microscope (MX-40, Olympus) and analyzed with the software ImageJ (NIH). The experimental λ_{max} of EHD is defined as the interplanar distance between the pillars in a hexagonal array, as illustrated in Figure 1a. To quantify λ_{max}, we performed a fast Fourier transform (FFT) on the microscopic image (Figure 1b). The six distinctive spots around the center in Figure 1b suggest a hexagonal order, and the small spot sizes implies uniformity in period.

THEORETICAL MODEL

The pillars in EHD form through a balance between the electrostatic, capillary and viscous forces. The growth is promoted by the applied voltage, which generates a Maxwell stress that is opposed by the capillary pressure from the surface tension. The rate of pillar growth is controlled by the viscous flow in the polymer layer. The relationship between these forces and the thickness of the polymer layer (h) is generated by solving the momentum and mass balances with the stress balance, no slip, and no penetration conditions at the interfaces. A linear stability analysis using the thickness $h = h_0 + \hat{h}(z, t)e^{ik\cdot x}$, with subscript o the base state, superscript hat the small periodic perturbation at interface, x and z the lateral and vertical coordinates, respectively, and $k = 2\pi/\lambda$ the wave vector (Figure 2), determines the growth rates of the Fourier components of the interface in terms of the growth exponent[1] M for perfect dielectrics as

$$\frac{d\hat{h}}{dt} = \frac{\varepsilon_0 V^2(\sinh(kh_0)\cosh(kh_0) - kh_0)}{2\eta_1(k^2h_0^2 + \cosh^2(kh_0))}[\{\varepsilon_1\varepsilon_2(\varepsilon_1 - \varepsilon_2)^2H\}/\{(\varepsilon_2\tanh(kh_0) + \varepsilon_1\tanh(k(H - h_0)))(\varepsilon_2h_0 + \varepsilon_1(H - h_0))^2\} - kL^2/H^2]\hat{h} \equiv M\hat{h} \quad (1)$$

with $L = (\gamma H^3/\varepsilon_0V^2)^{1/2}$ the characteristic lateral length scale, ε_0 the vacuum permittivity, and η_1 the polymer viscosity. The lubrication approximation is not invoked because $H/L \sim O(1)$ for submicrometer features.

The theoretical λ_{max} is the wavelength with the largest growth exponent (M_{max}). For a polymer−air bilayer, reduction of λ_{max} can be achieved through increasing h_0 (since $\varepsilon_2 < \varepsilon_1$) and V or decreasing H. On the other hand, a smaller surface tension (γ), larger dielectric constant of the top layer (ε_2), and/or larger conductivity (σ) also decrease λ_{max}. By possessing all of these properties, IL is a good choice to replace air in the gap.

In a polymer−IL bilayer, the Poisson equation governs the potential in the polymer layer (eq 2a). On the other hand, given that the IL ions diffuse much faster than the alternating rate of our applied voltage, the ionic liquid is fully polarized and its potential (ψ_2) is pseudo-steady. Therefore, the IL potential is governed by both the Poisson and the ion conservation equation at steady state (eq 2b).[21] The boundary conditions are the grounded and applied potentials at the bottom and top electrodes, respectively, the continuity of dielectric displacement vector and potential at the polymer−IL interface, and no ion fluxes

across the two interfaces adjacent to the IL layer (eq 2c)

$$\varepsilon_0\varepsilon_1\nabla^2\psi_1 = 0 \quad \text{for} \quad 0 \le z \le h_0 \tag{2a}$$

$$\varepsilon_0\varepsilon_2\nabla^2\psi_2 = -2en' \quad \text{and} \quad \nabla^2\psi_2 = -\frac{k_BT}{en^\infty}\nabla^2 n' \quad \text{for } h_0 \le z \le H \tag{2b}$$

$$\psi_1 = 0 \quad \text{at } z = 0$$

$$\varepsilon_0\varepsilon_1 E_1 = \varepsilon_0\varepsilon_2 E_2 \quad \text{and} \quad \psi_1 = \psi_2 \quad \text{and} \quad \nabla\psi_2 = -\frac{k_BT\nabla n'}{en^\infty} \quad \text{at } z = h_0$$

$$\psi_2 = V \quad \text{and} \quad \nabla\psi_2 = -\frac{k_BT\nabla n'}{en^\infty} \quad \text{at } z = H \tag{2c}$$

with e the electronic charge, k_B the Boltzmann constant, n^∞ and n' the bulk and perturbed ion concentrations, respectively, and E_1 and E_2 the electric fields in the polymer and IL layer at the interface, respectively.

The linearization as $\psi = \psi_0 + \hat{\psi}(z,t)e^{ik\cdot x}$ and the assumption that $\hat{h}$ is very small leads to base and perturbed states of the IL potential at the polymer−IL interface (h) as

$$\psi_{2o} \approx \frac{V\varepsilon_2 h_0\kappa}{2\varepsilon_1 + \varepsilon_2 h_0\kappa} \quad \text{and}$$

$$\hat{\psi}_2 \approx \frac{V\varepsilon_1\varepsilon_2\kappa(k + (\alpha - \kappa)\tanh(kh_0))}{(2\varepsilon_1 + \varepsilon_2 h_0\kappa)(\varepsilon_1 k + \varepsilon_2\alpha\tanh(kh_0))} \tag{3}$$

with $\kappa = [(2e^2n^\infty)/(\varepsilon_0\varepsilon_2 k_BT)]^{1/2}$ the inverse Debye length and $\alpha^2 = (k^2 + \kappa^2)$.

Finally, a linear stability analysis determines λ_{max} with a negligible IL viscosity ($\eta_2/\eta_1 \approx 10^{-8}$) as mentioned before. The conservation of lateral and normal momentum relates the pressure P to the lateral and normal velocities w and u. Mass balance provides the third independent equation leading to a fourth-order differential equation in the vertical velocity in polymer u_1 as expressed in eq 4a, with boundary conditions from the stress balance, no slip, and no penetration conditions at interfaces (eq 4b)

$$\frac{d^4\hat{u}_1}{dz^4} - 2k^2\frac{d^2\hat{u}_1}{dz^2} + k^4\hat{u}_1 = 0 \tag{4a}$$

$$\frac{d^3\hat{u}_1}{dz^3} - \frac{3k^2\varepsilon_0{}^2V^4H^2}{\eta_1{}^2L^4}\frac{d\hat{u}_1}{dz} = \frac{k^2\varepsilon_0{}^3V^6}{\eta_1{}^3L^2H}\left[\frac{\varepsilon_2(\varepsilon_2 - \varepsilon_1)H^3}{\varepsilon_1L^2V^2}E_{2o}\hat{E}_2 + k^2\hat{h}\right]$$

$$\text{and} \quad \frac{d^2\hat{u}_1}{dz^2} + k^2\hat{u}_1 = 0 \quad \text{at } z = h_0 \tag{4b}$$

$$\frac{d\hat{u}_1}{dz} = 0 \quad \text{and} \quad \hat{u}_1 = 0 \quad \text{at } z = 0$$

with E_{2o} and $\hat{E}_2$ the base and perturbed electric fields in IL at the interface.

Given that $\kappa H \sim O(10^3)$ for our experimental conditions, we can then approximate the time-averaged perturbed interfacial height as

$$\frac{d\hat{h}}{dt} \approx \frac{\varepsilon_0V^2[\sinh(kh_0)\cosh(kh_o) - kh_0]}{2\eta_1[(k^2h_0)^2 + \cosh^2(kh_0)]}\left[\frac{\varepsilon_1(\varepsilon_2 - \varepsilon_1)H}{2\varepsilon_2h_0{}^2\tanh(kh_0)} - \frac{kL^2}{H^2}\right]\hat{h} \equiv M\hat{h} \tag{5}$$

For a given polymer and ionic liquid (where ε_1, ε_2, and γ are fixed), we find λ_{max} to be relatively insensitive to changes in H but reducible by decreasing h_0 and/or increasing V. With typical parameters (h_0 = 17 nm, H = 88 nm, and V = 5 V), λ_{max} decreases by more than an order of magnitude with the introduction of ionic liquid, from 6.43 μm to 148 nm, which is comfortably submicrometer.

RESULTS AND DISCUSSION

1. Polymer−Air Bilayer. Consistent with previously reported experimental λ_{max} for a polymer−air bilayer,[19] we found little decrease below 1 μm even when expected from the model (Figure 3a). In fact, for experiments at $||V|| \ge 30$ V, we observed λ_{max} larger than the theoretical value and relatively constant at about 2 μm. Furthermore, the experimental variability within each sample was generally larger than with lower voltages as indicated by the error bars that show the standard deviations. On the contrary, experiments at $||V|| \le 20$ V produced λ_{max} smaller than predicted from the perfect dielectric model as shown in eq 1. We attribute both deviations from the theoretical values to the dielectric breakdown of the layers, which occurs when the expected electric field (E_{exp}) exceeds the dielectric field strength of the material. Upon dielectric breakdown, a medium no longer behaves as a perfect insulator and starts to conduct electricity.

The dielectric field strengths of PMMA and air at submicrometer thickness as reported in the literature range from 0.045 to 0.11 V nm^{-1} [22−25] and 0.029 to 0.175 V nm^{-1},[26−29] respectively. Considering the lower limit of the literature value as the dielectric strength, we expect that the air layer has broken down in all experiments ($E_{exp} \ge 0.029$ V nm^{-1}) and that the PMMA layer has broken down only in experiments at $||V|| \ge 30$ V ($E_{exp} \ge 0.061$ V nm^{-1}).

For $||V|| \le 20$ V, air seems to break down while PMMA remains a perfect dielectric ($E_{exp} \le 0.041$ V nm^{-1}). The leaky dielectric model in Pease and Russel[1] should hold, but with mobile charges from the discharge accumulating at the air side of the interface instead of the PMMA side (details are provided in Supporting Information). In addition to the momentum and mass balances, the governing equations also include charge conservation. The theoretical λ_{max}, assuming a high conductivity σ such that $(\sigma\eta_1\gamma H^3)/(\varepsilon_0{}^3\varepsilon_2{}^3V^4) \gg 1$, plotted as the dashed line in Figure 3a suggests that the leaky dielectric model predicts the direction of the shift in λ_{max} for $||V|| \le 20$ V. However, the experimental λ_{max} consistently exceeds the theoretical value from the leaky dielectric model, presumably because air is neither a perfect dielectric nor a perfect conductor upon breakdown.

For samples at $||V|| \ge 30$ V, we expect dielectric breakdown in both layers. Gross treated such systems as a polymer−air two-layer capacitor with the field in each layer limited by the dielectric field strength (E_b).[30] Above E_b, Gross suggested that dielectric breakdown will occur through discharges to reduce the areal charge in the broken down layer to $\varepsilon_0\varepsilon E_b$. Since the thickness of each layer is roughly the same throughout our experiments, the effective voltage due to discharge ($V_{eff} = E_bh_0$) will be constant but lower than the expected value without breakdown, producing a relatively constant λ_{max} larger than the theoretical value from the perfect dielectric model (eq 1). Furthermore, the larger variability in these experiments, as indicated by the error bars, was likely due to the local degradation caused by the discharges.

Although increasing h_0 and/or decreasing H should decrease λ_{max}, our model suggests that the voltage required to obtain submicrometer features will result in dielectric breakdown in at least one of the layers independent of h_0 and/or H. If both

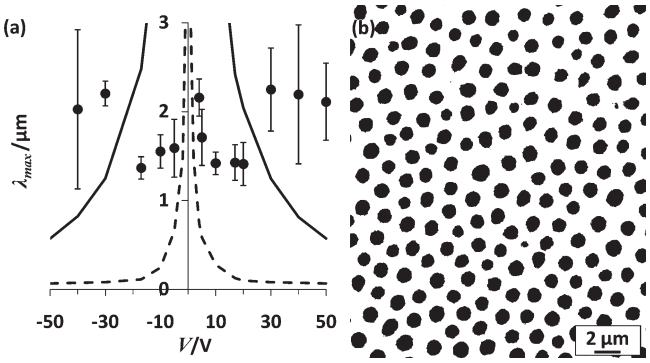

Figure 3. EHD of PMMA2K−air at h_0 = 48 nm, H = 171 nm, and T = 130 °C. (a) Plot of λ_{max} vs applied voltage, with solid and dashed lines indicating the values of λ_{max} from a perfect dielectric model and a leaky dielectric model ($(\sigma\eta_1\gamma H^3)/(\varepsilon_0{}^3\varepsilon_2{}^3V^4) \gg 1$), respectively. (b) An optical micrograph of pillars formed at 10 V, at which dielectric breakdown in air layer caused lower degree of ordering.

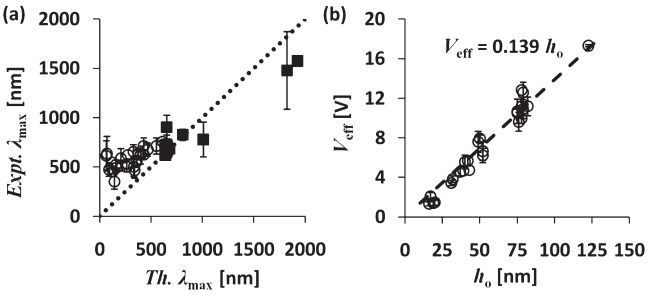

Figure 4. (a) Plot of experimental vs theoretical λ_{max} of PS77K-IL bilayer with a range of conditions. Solid squares (■) indicate experiments with $E_{exp} \leq 0.139$ V nm^{-1}, and open circles (○) indicate experiments with $E_{exp} \geq 0.158$ V nm^{-1}. Dotted line indicates the expected unit slope. (b) Plot of effective voltages (V_{eff}) deduced from the positively deviated λ_{max} (○) in (a) against their polymer thicknesses (h_0).

layers break down, submicrometer features are unlikely. Even if only one layer breaks down, the pillars seem to be less ordered (Figure 3b) than those formed with perfect dielectrics (Figure 1a). Therefore, we cannot achieve ordered submicrometer features with a polymer−air bilayer.

While we agree with Pease and Russel[31] that air breakdown contributes to the limitation, dielectric breakdown in polymer is also important, as supported by more recent publications on the dielectric field strength of PMMA thin films.[22−25] Dielectric breakdown in both layers explains the relatively constant λ_{max} at high applied voltages reported by both Pease and Russel[31] and this paper. We also show that dielectric breakdown leads to larger variation in λ_{max} and disruption of pillar ordering.

2. Polymer−Ionic Liquid Bilayer. Several issues arose with the use of an ionic liquid in the gap. Our first attempt with a spin-coated PMMA film under a PMMA63K−IL bilayer detached from the silicon wafer after the experiment. The situation worsened upon removing the IL by rinsing the system gently. This could indicate a higher affinity of PMMA for BMI-BF_4 than silicon. Since previous studies with PMMA[3,4,6] and PS[5,6,32] have produced very similar EHD patterns with a flat mask and an air gap, we switched to BMI-BF_4 with PS77K, which eliminated the problems.

We also encountered oxidation of the IL which appeared as a brown precipitate upon applying a constant voltage[33] even within the electrochemical window (∼2.45 V[34]). Fortunately, switching to an alternating voltage eliminated the problem, consistent with the observation in Lozano et al.,[33] suggesting that the oxidation of the ionic liquid is time-dependent.

Finally, we observed a minute amount of ionic liquid leaking out of the gap, thereby establishing direct contact between the top electrode and the larger polymer film across the oxide layer. Therefore, we decided to neglect the voltage drop across the oxide.

With this strategy, we achieved features smaller than with a PS77K−air bilayer over a wide range of experimental conditions. The smallest λ_{max} was 351 ± 78 nm. Figure 4a shows that λ_{max} observed agrees relatively well with theory from the PS−IL model at the larger wavelengths but deviates below about 650 nm. Additionally, the expected fields across the PS in experiments that produced the smaller, yet still positively deviated, λ_{max} (○) were at least 0.158 V nm^{-1}, while those associated with larger λ_{max} (■) did not exceed 0.139 V nm^{-1}. To determine whether this deviation was due to dielectric breakdown of PS, we deduced from the PS−IL model (eq 5) the effective voltage across the polymer film (V_{eff}) from the measured λ_{max}. The V_{eff} from a large range of polymer thicknesses h_0 plotted in Figure 4b show a linear increase with h_0, which agrees with dielectric breakdown at a characteristic field limiting the maximum sustainable voltages. The slope of the plot suggests the dielectric field strength of PS to be 0.139 ± 0.026 V nm^{-1}, which falls within the range of literature values (0.02−0.40 V nm^{-1}).[35,36]

The effective electric fields ($E_{eff} = V_{eff}/h_0$) of all samples were then plotted against their respective E_{exp} in Figure 5. For experiments with E_{exp} smaller than the dielectric field strength deduced from Figure 4b (0.139 ± 0.026 V nm^{-1}), E_{eff} should agree with E_{exp} since no breakdown has occurred. This was supported by the solid squares (■), which fall about the dotted line with unit slope. However, for E_{exp} exceeding 0.139 ± 0.026 V nm^{-1}, dielectric breakdown should limit E_{eff} to a constant field strength through discharging. The open circles (○), as discussed in Figure 4b, fall around the deduced dielectric field strength of 0.139 ± 0.026 V nm^{-1} (- - -) for $h_0 \geq 31$ nm. Furthermore, the dielectric field strength seems to be smaller for ultrathin films ($h_0 \leq 20$ nm), with the crosses (×) suggesting a limiting field strength of 0.088 ± 0.023 V nm^{-1} (- · -). The smaller strength for ultrathin polymer films is consistent with reports in the literature.[37]

Though λ_{max} can be decreased with a larger voltage and/or a thinner polymer film in a polymer−IL bilayer, both increase the tendency of dielectric breakdown in polymer, especially for ultrathin films ($h_0 \leq 20$ nm) which have a smaller dielectric strength. Therefore, our results suggest that the limiting dielectric strength of the polymer constrains the further reduction in feature size, preventing the achievement of 10 nm features as expected by others.[38]

We also observed that the pillars produced with a PS−IL bilayer (Figure 6b) were more disordered and polydisperse in sizes than those with a PS−air bilayer (Figure 6a). Both samples were obtained at alternating electric fields below the deduced dielectric field strength, thus eliminating discharge as a factor. Coarsening is also unlikely to be the cause for poor patterning since Wu et al. showed that the majority of coarsening starts after a dimensionless experimental time, scaled on $M_{max}{}^{-1}$, around 100 for $h_0/H \leq 0.46$.[39] Most of our experiments had smaller dimensionless times (≤18) and small to intermediate h_0/H (≤0.52), both of which retard the onset of coarsening as

dx.doi.org/10.1021/ma200952u |*Macromolecules* 2011, 44, 7746–7751

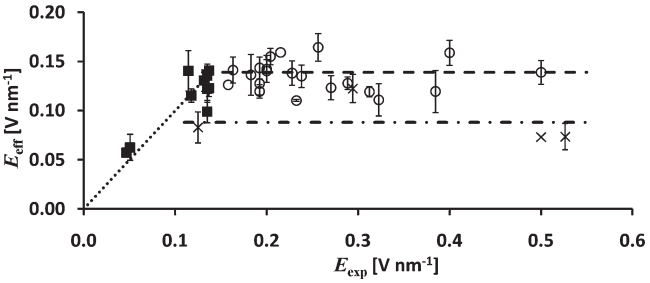

Figure 5. Plot of effective electric field vs expected field. Solid squares (■) correspond to experiments with $E_{exp} \leq 0.139$ V nm^{-1} and $h_0 \geq 31$ nm, open circles (○) correspond to experiments with $E_{exp} \geq 0.158$ V nm^{-1} and $h_0 \leq 31$ nm, and crosses (×) correspond to experiments with $E_{exp} \geq 0.125$ V nm^{-1} and $h_0 \leq 20$ nm. Dotted line (···) has a slope of 1, dashed line (- - -) indicates $E_{eff} = 0.139$ V nm^{-1}, and dash-dot line (- · -) indicates $E_{eff} = 0.088$ V nm^{-1}.

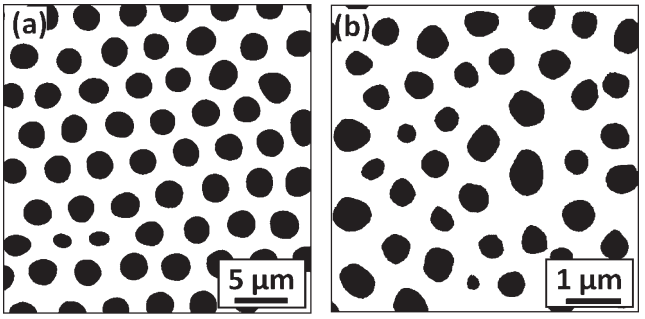

Figure 6. Optical micrographs of pillars formed from electrohydrodynamic patterning on (a) a polystyrene−air bilayer and (b) a polystyrene−ionic liquid bilayer.

suggested by Wu et al.[39] and Verma et al.[40] Furthermore, if coarsening is significant, we would expect the range of the dielectric field strength deduced from the model to be broader. These suggest that the dispersed pillar sizes and poor order arise before major coarsening begins. The roughly six nearest neighbors also imply that coarsening through collision,[39] which decreases the number of nearest neighbors, had not occurred. Perhaps "Ostwald ripening"[39] had just started, which would increase the polydispersity in pillar sizes but leave λ_{max} unchanged.

Since the poor patterns were observed in all PS−IL experiments regardless of the dimensionless time, h_0/H, and V, the fluid−fluid interface seems to be the culprit. This is consistent with previous studies on EHD of various polymers with a flat mask. While poly(methyl methacrylate),[3,4] polystyrene,[5,32] and polyisoprene[9] form more monodisperse and well-ordered pillars with an air gap, their patterns with another oligomer[9] or polymer[11] in the gap are generally polydisperse and disordered. However, the exact explanation is yet to be determined.

CONCLUSIONS

Electrohydrodynamic patterning (EHD) of a polymer−air bilayer with a flat mask commonly produces ordered pillar arrays with feature sizes (λ_{max}) of several micrometers. While trying to access smaller scales, we observed a limitation due to dielectric breakdown along with a lower degree of pillar ordering. We demonstrate that λ_{max} from EHD on a polymer film can be reduced to the submicrometer scale, as small as 351 ± 78 nm, with a polymer−ionic liquid bilayer. Though theory predicts that thinner polymer films (h_0) and higher voltages (V) will decrease λ_{max}, the limit is set by the dielectric field strength of the polymer. In addition, the limiting field strength also seems to decrease in ultrathin films (≤20 nm), further restricting feature size reduction.

ASSOCIATED CONTENT

Supporting Information. Equations of the leaky dielectric model for the polymer−ionic liquid bilayer. This material is available free of charge via the Internet at http://pubs.acs.org.

AUTHOR INFORMATION

Corresponding Author
*E-mail: wbrussel@princeton.edu.

ACKNOWLEDGMENT

This work was supported by the MRSEC Grant at Princeton University NSF DMR 0819860.

REFERENCES

(1) Pease, L. F.; Russel, W. B. *J. Chem. Phys.* **2003**, *118*, 3790–3803.
(2) Bandyopadhyay, D.; Sharma, A. *J. Colloid Interface Sci.* **2007**, *311* (2), 595–608.
(3) Wu, N. Nonlinear Dynamics of Pattern Formation via Electrohydrodynamic Instabilities. PhD Thesis, Princeton University, Princeton, NJ, 2008.
(4) Chou, S. Y.; Zhuang, L.; Guo, L. *Appl. Phys. Lett.* **1999**, *75* (7), 1004–1006.
(5) Schäffer, E.; Thurn-Albrecht, T.; Russell, T. P.; Steiner, U. *Nature* **2000**, *403*, 874–877.
(6) Schäffer, E.; Thurn-Albrecht, T.; Russell, T. P.; Steiner, U. *Europhys. Lett.* **2001**, *53* (4), 518–524.
(7) Dickey, M.; Raines, A.; Collister, E.; Bonnecaze, R.; Sreenivasan, S.; Willson, C. *J. Mater. Sci.* **2008**, *43* (1), 117–122.
(8) Zhuang, L. Controlled Self-Assembly in Homopolymer and Diblock Copolymer. PhD Thesis, Princeton University, Princeton, NJ, 2002.
(9) Lin, Z.; Kerle, T.; Baker, S. M.; Hoagland, D. A.; Schäffer, E.; Steiner, U.; Russell, T. P. *J. Chem. Phys.* **2001**, *114* (5), 2377–2381.
(10) Bae, J.; Glogowski, E.; Gupta, S.; Chen, W.; Emrick, T.; Russell, T. P. *Macromolecules* **2008**, *41* (7), 2722–2726.
(11) Lin, Z.; Kerle, T.; Russell, T. P.; Schäffer, E.; Steiner, U. *Macromolecules* **2002**, *35* (10), 3971–3976.
(12) Benisty, H.; Olivier, S.; Weisbuch, C.; Agio, M.; Kafesaki, M.; Soukoulis, C. M.; Qiu, M.; Swillo, M.; Karlsson, A.; Jaskorzynska, B.; Talneau, A.; Moosburger, J.; Kamp, M.; Forchel, A.; Ferrini, R.; Houdré, R.; Oesterle, U. *IEEE J. Quantum Electron.* **2002**, *38* (7), 770–785.
(13) Vukusic, P.; Sambles, J. R. *Nature* **2003**, *424* (6950), 852–855.
(14) Barthlott, W.; Neinhuis, C. *Planta* **1997**, *202* (1), 1–8.
(15) Li, B.; Fang, X.; Luo, H.; Seo, Y.-S.; Petersen, E.; Ji, Y.; Rafailovich, M.; Sokolov, J.; Gersappe, D.; Chu, B. *Anal. Chem.* **2006**, *78* (14), 4743–4751.
(16) Chan, Y. C.; Lee, Y.-K.; Zohar, Y. In Pillar size effect on DNA electrophoresis in microchips with sub-micron pillar arrays. *20th IEEE Int. Conf. Micro Electro Mech. Syst., 21−25 Jan. 2007*, 2007; pp 413−416.
(17) Lei, X.; Wu, L.; Deshpande, P.; Yu, Z.; Wu, W.; Ge, H.; Chou, S. Y. *Nanotechnology* **2003**, *14* (7), 786–790.
(18) Wu, N.; Pease, L. F.; Russel, W. B. *Adv. Funct. Mater.* **2006**, *16* (15), 1992–1999.
(19) Pease, L. F.; Russel, W. B. *Langmuir* **2003**, *20* (3), 795–804.

(20) *Polymer Data Handbook*, online ed.; Oxford University Press.
(21) Hollingsworth, A. D.; Saville, D. A. *J. Colloid Interface Sci.* **2003**, *257* (1), 65–76.
(22) Na, M.; Rhee, S.-W. *Org. Electron.* **2006**, *7* (4), 205–212.
(23) Miyairi, K.; Itoh, E. In AC electrical breakdown and conduction in PMMA thin films and the influence of LiClO4 as an ionic impurity. *Proc. IEEE Int. Conf. Solid Dielectr., 5−9 July 2004*, 2004; Vol. *1*, pp 99−102.
(24) Lyuksyutov, S. F.; Vaia, R. A.; Paramonov, P. B.; Juhl, S.; Waterhouse, L.; Ralich, R. M.; Sigalov, G.; Sancaktar, E. *Nature Mater.* **2003**, *2* (7), 468–472.
(25) Park, J. H.; Hwang, D. K.; Lee, J.; Im, S.; Kim, E. *Thin Solid Films* **2007**, *515* (7−8), 4041–4044.
(26) Torres, J. M.; Dhariwal, R. S. *Microsyst. Technol.* **1999**, *6* (1), 6–10.
(27) Slade, P. G.; Taylor, E. D. *IEEE Trans. Compon. Packag. Technol.* **2002**, *25* (3), 390–396.
(28) Wallash, A.; Levit, L. *Proc. SPIE* **2003**, *4980*, 87–96.
(29) Hourdakis, E. S. Electrical measurements at the microscale: Air breakdown and silicon Coulomb blockade devices. PhD Thesis, University of Maryland, 2007.
(30) Gross, B. *Br. J. Appl. Phys.* **1950**, *1* (10), 259–267.
(31) Pease, L. F.; Russel, W. B. *Langmuir* **2004**, *20* (3), 795–804.
(32) Voicu, N. E.; Harkema, S.; Steiner, U. *Adv. Funct. Mater.* **2006**, *16* (7), 926–934.
(33) Lozano, P.; Martínez-Sánchez, M. *J. Colloid Interface Sci.* **2004**, *280* (1), 149–154.
(34) Xiao, L.; Johnson, K. E. *J. Electrochem. Soc.* **2003**, *150* (6), E307–E311.
(35) Prime, D.; Paul, S. *Vacuum* **2010**, *84* (10), 1240–1243.
(36) Hikita, M.; Matsuda, A.; Nagao, M.; Sawa, G.; Ieda, M. *Jpn. J. Appl. Phys.* **1982**, *21* (Part 1, No. 3), 475−482.
(37) Prime, D. C. Switching Mechanisms, Electrical Characterisation and Fabrication of Nanoparticle Based Non-Volatile Polymer Memory Devices. PhD Thesis, Emerging Technologies Research Centre, De Montfort University, 2010.
(38) Goldberg-Oppenheimer, P.; Steiner, U. *Small* **2010**, *6* (11), 1248–1254.
(39) Wu, N.; Kavousanakis, M. E.; Russel, W. B. *Phys. Rev. E* **2010**, *81* (2), 026306.
(40) Verma, R.; Sharma, A.; Kargupta, K.; Bhaumik, J. *Langmuir* **2005**, *21* (8), 3710–3721.

■ NOTE ADDED AFTER ASAP PUBLICATION

This article posted ASAP on August 30, 2011. Equations 4b and 5 have been reformatted. The correction version reposted on September 7, 2011.